Supplemental Information

Interconnected Silicon-Carbon Conductive Framework Dissipating Mechanical Strain for Advanced Li-ion Storage

Shengsong Li[a], Gengyi Wang[a], Tao Meng[a*], Aimei Gao[a,b], Fenyun Yi[a,b], Shanqiang Ou[c], Bo Li[d], Cong Liu[c], Dong Shu[a,b*], Yexiang Tong[c]

[a] School of Chemistry, South China Normal University, Guangzhou 510006, P. R. China

[b] National and Local Joint Engineering Research Center of MPTES in High Energy and Safety LIBs, South China Normal University, Guangzhou 510006, P. R. China

[c] MOE of the Key Laboratory of Bioinorganic and Synthetic Chemistry, The Key Lab of Low-Carbon Chemistry & Energy Conservation of Guangdong Province, School of Chemistry, Sun Yat-sen University, Guangzhou 510275, P. R. China

[d] Guizhou Provincial Key Laboratory of Computational Nano-Material Science, Guizhou Education University, Guiyang, Guizhou 550018, P. R. China

* Corresponding author: dshu@scnu.edu.cn; mengt@scnu.edu.cn

Experimental section

Materials preparation

All chemicals were of analytical grade and used without further purification. The Si@SiO_x powder (98% purity, diameter < 50 nm) was purchased from Alfa Aesar. Polyvinyl alcohol (PVA) and ammonium thiosulfate ($(NH_4)_2S_2O_3$, > 99%) were purchased from Shanghai McLean biochemical Co., Ltd.

Preparation of Si@C composites: Uniform viscous solution was obtained by dissolving 0.18 g PVA powder in 15 mL distilled water. 0.2 g Si@SiO_x powder was dispersed into the mixture of PVA solution and distilled water (10 mL), and then stirred evenly 0.1 g $(NH_4)_2S_2O_3$ was dissolved in an appropriate amount of distilled water and added to the mixture. Then, the mixture was sonicated for half an hour to ensure uniform mixing. The mixture was quickly transferred to the refrigerator to freeze overnight, then used the freeze dryer to dry at -65 °C for 24 h. Finally, the dried material was transferred to a tube furnace and calcined at 600 ℃ in nitrogen for 4 hours at a heating rate of 2 °C min^{-1}. The obtained product was denoted as FNS-Si@C. As a contrast, NS-Si@C was prepared by blast drying at 65 °C for 3 hours and other synthesis processes were the same. Si@C was prepared by blast drying without $(NH_4)_2S_2O_3$ and other synthesis processes were the same.

Material characterization

The morphology and cross-sectional properties of the samples were characterized by scanning electron microscope (Gemini 500) and transmission electron microscope (FEI F30). The crystal structure of the samples was analyzed by X-Ray Powder diffractometer (XRD, UltimaIV) in the 2θ range of 5-80° at scan rate of 10° min^{-1}. Raman analysis was performed by Renishaw inner hole Raman microscope (λ= 633 nm). The functional groups of PVA and Si@SiO_x were detected by Fourier transform infrared spectroscopy (Nicolet 6700 Thermo Science). Thermogravimetric analysis (TG209F3) was carried out in air atmosphere from room temperature to 700 °C. The specific surface area and pore volume of the samples were measured by nitrogen

adsorption/desorption (BET, ASAP-2020). The chemical state and elemental analysis of the samples were studied by X-ray photoelectron spectroscopy (ESCALab250Xi). The surface potential of the sample was measured by Kelvin microscope (SPM9500J3). The contact angle between material and electrolyte was measured on SDC-100 contact angle tester.

Electrochemical measurement

The prepared composites were used as anode materials, and the electrochemical performance of the prepared electrodes were evaluated by CR2032 coin half cells and full cells. When preparing the electrode, the active material, binder (sodium alginate) and acetylene black were mixed in an appropriate amount of deionized water according to the weight ratio of 7:2:1, and a uniform slurry was obtained. The slurry was evenly coated on the copper foil with a scraper and dried in a vacuum oven at 65 °C overnight. The electrode film was punching into discs with the diameter of 12 mm. The electrolyte is composed of 1 M $LiPF_6$/EC/DMC (v/v=1:1) and 5 wt% fluorinated ethylene carbonate (FEC) additive, The amount of electrolyte used in a coin battery is about 60 μL. The metallic Li and Celgard 2400 were used as counter electrodes and separator respectively. The mass loading of active material was about 0.5-1.0 mg cm^{-2}. The cells were assembled in a glove box filled with Ar (H_2O, O_2 < 0.1 ppm) and then aged for at least 24 h before electrochemical performance tests were carried out.

For the full cell, the coin-type and pouch cell were assembled with commercial $LiFePO_4$ and FNS-Si@C as cathode and anode respectively. The anode was prelithiated to compensate for the first irreversible lithium loss by adding a few drops of electrolyte on the FNS-Si@C electrode and pressing 20 min with Li foil. The mass ratio of cathode and anode was set to 10.5:1, which was based on the total weight of the active material to calculate the specific capacity of the full cell.

The galvanostatic charge/discharge and discharge was carried out on the LAND2001a battery tester. The cyclic voltammograms were performed on the CHI660E electrochemical workstation. Electrochemical impedance spectroscopy (EIS) was conducted by CHI660E electrochemical workstation (10^{-2}-10^{-6} Hz).

Theoretical calculation

The interaction energy between PVA and SiO_2 obtained by M06-2X-D3/def2svp level and Gaussin16 package (Revision C.01).[1-4] The interaction energy was calculated as follows:

$$E_{\text{int-PVA-SiO}_2} = E_{\text{PVA-SiO}_2} - E_{\text{PVA}} - E_{\text{SiO}_2} \quad \text{(Equation S1)}$$

KPFM measures the surface potential of materials

In the KPFM tip mode measurement, the work function can be expressed as:

$$\varphi_s = \varphi_{tip} - \Delta\varphi \quad \text{(Equation S2)}$$

Here φ_s is the work function of sample, φ_{tip} is the work function of the gold tip, which is already known, and $\Delta\varphi$ is the offset voltage. During measurement, the φ_{tip} is the same, so the change of work function (φ_s) could be acquired from the change of $\Delta\varphi$.[5]

Calculation of Li^+ diffusion coefficient by cyclic voltammetry

$$I_p = 2.69 \times 10^5 n^{1.5} A D^{0.5} \text{Li}^+ \nu^{0.5} C_{\text{Li}^+} \quad \text{(Equation S3)}$$

where I_p is the peak current, n is the number of electrons in the reaction, A is the area of the electrode, ν is the scanning rate (V s^{-1}), C_{Li^+} is the Li-ion concentration in the electrolyte and D_{Li^+} is the Li-ion diffusion coefficient, The n, A and C_{Li^+} are constant.[6]

Capacitive and diffusion contributions using cyclic voltammetry curve

The capacitive contribution ($k_1 \nu$) and diffusion control contribution ($k_2 \nu^2$) are calculated from the CV curve of FNS-Si@C at different scanning rates, according to the equation S4:

$$i = k_1 \nu + k_2 \nu^{1/2} \quad \text{(Equation S4)}$$

where k_1 and k_2 are constants, i and ν corresponds to the peak current and scan rate.

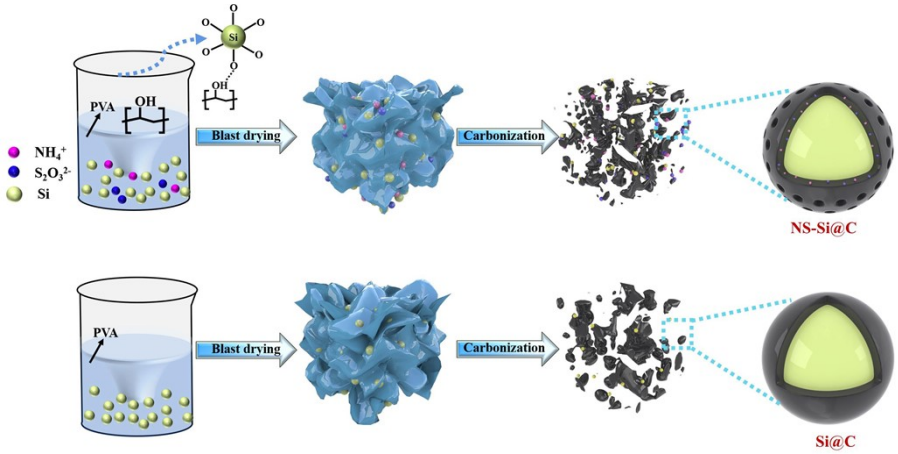

Figure S1. Synthesis process of the NS-Si@C and Si@C composites.

Figure S2. Digital images of various stages of blast drying.

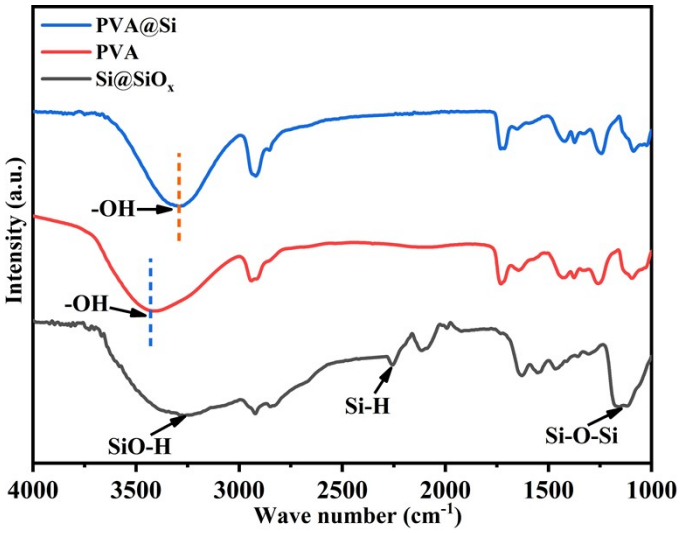

Figure S3. FTIR spectra of $Si@SiO_x$, PVA and Si@PVA.

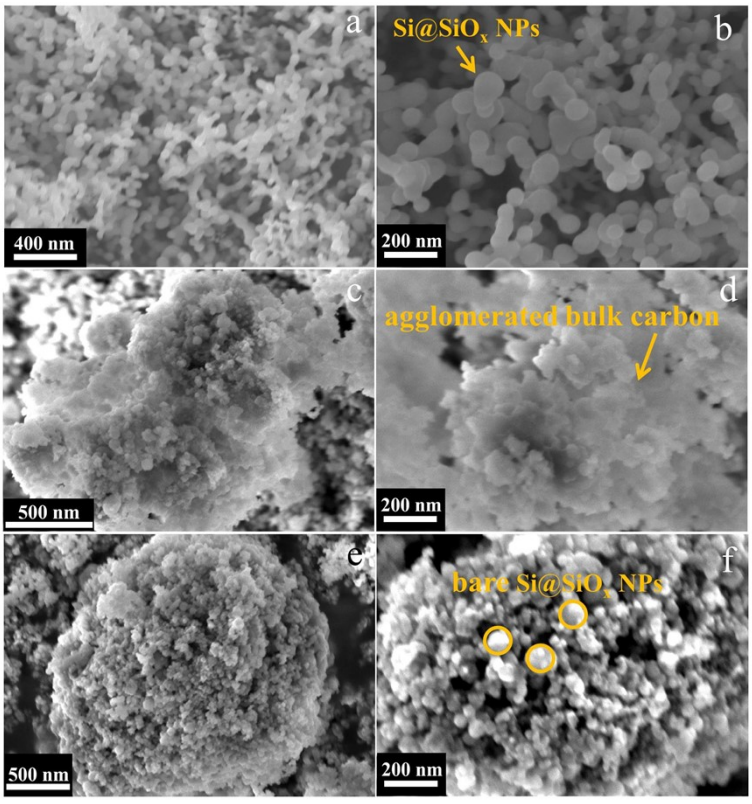

Figure S4. SEM images. (a, b) $Si@SiO_x$; (c, d) Si@C; (e, f) NS-Si@C.

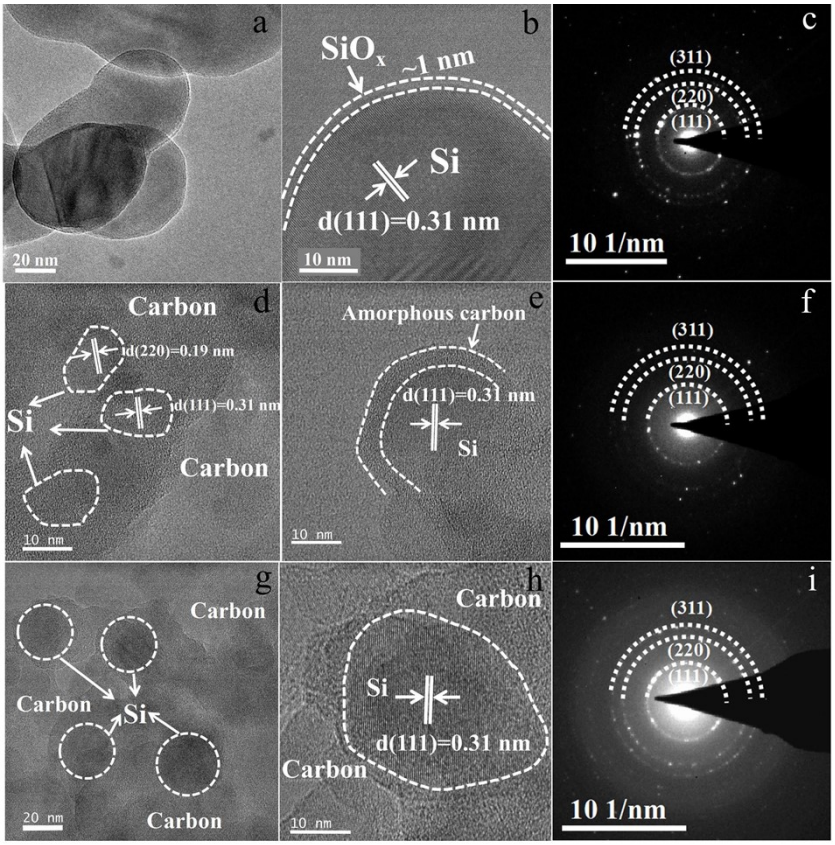

Figure S5. TEM images and SAED patterns. (a-c) Si@SiO_x; (d-f) Si@C; (g-i) NS-Si@C.

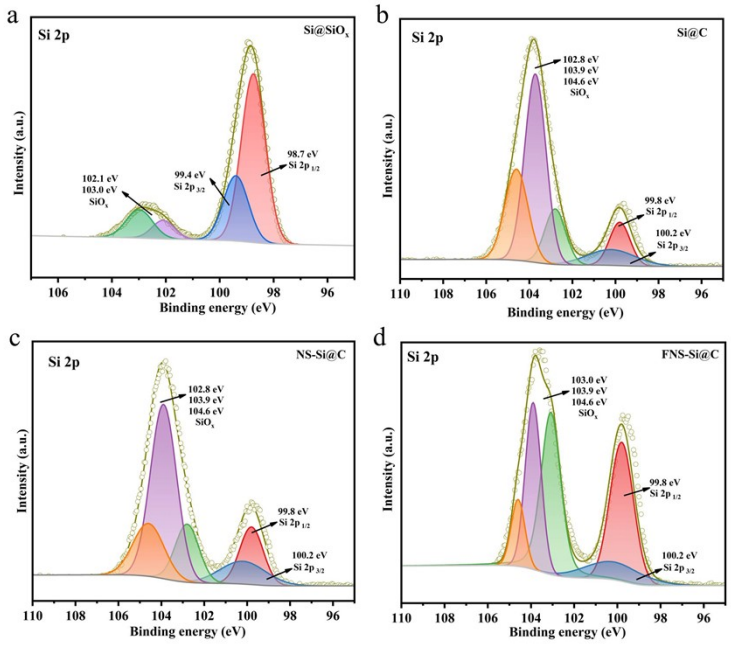

Figure S6. High-resolution XPS Si 2p spectrum. (a) Si@SiO_x, (b) Si@C, (c) NS-Si@C, (d) FNS-Si@C.

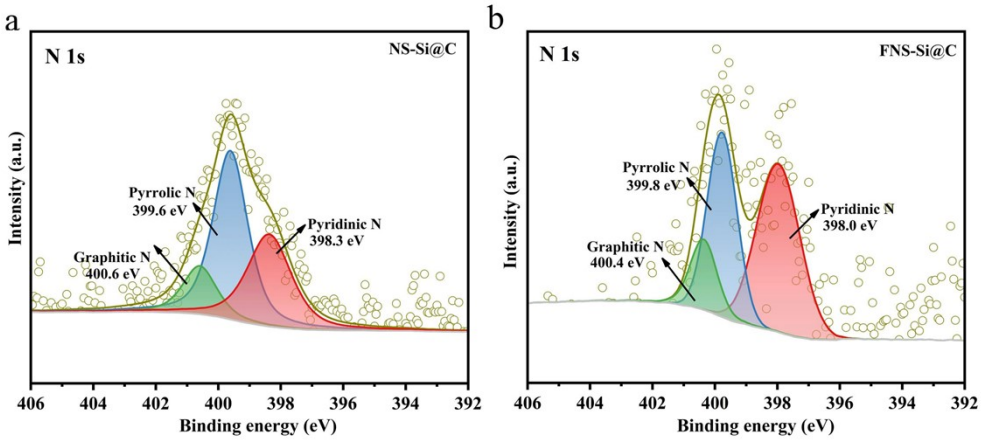

Figure S7. High-resolution XPS N 1s spectrum. (a) NS-Si@C; (b) FNS-Si@C.

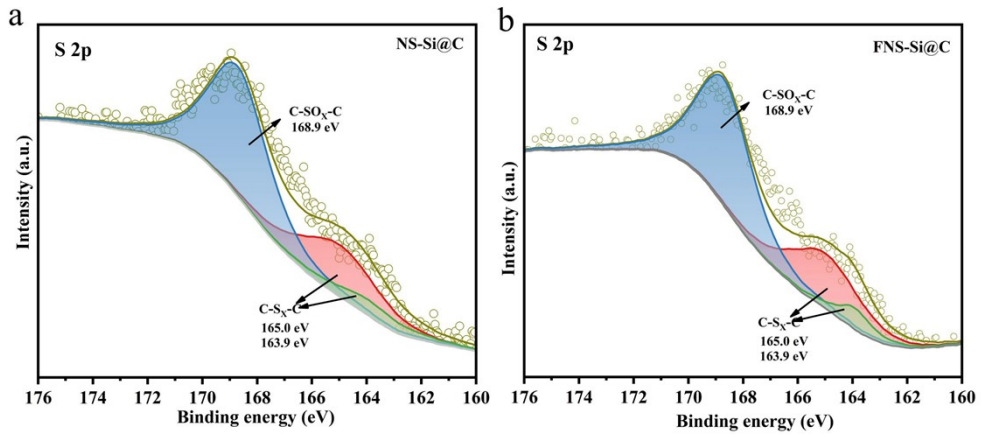

Figure S8. High-resolution XPS S 2p spectrum. (a) NS-Si@C; (b) FNS-Si@C.

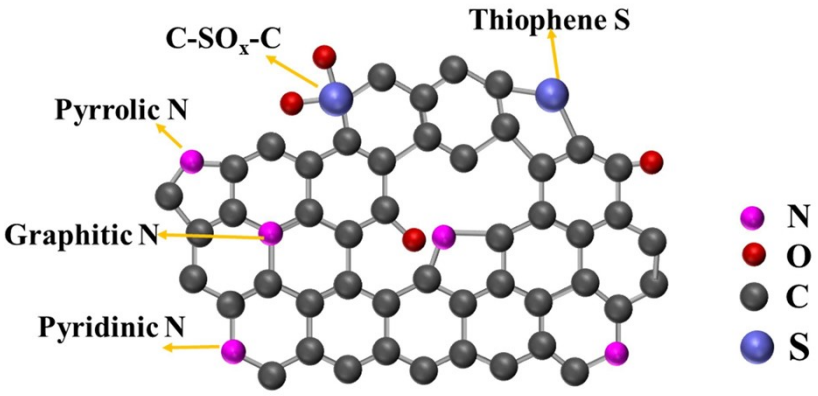

Figure S9. Schematic of nitrogen and sulfur functionalities in the carbon skeleton.

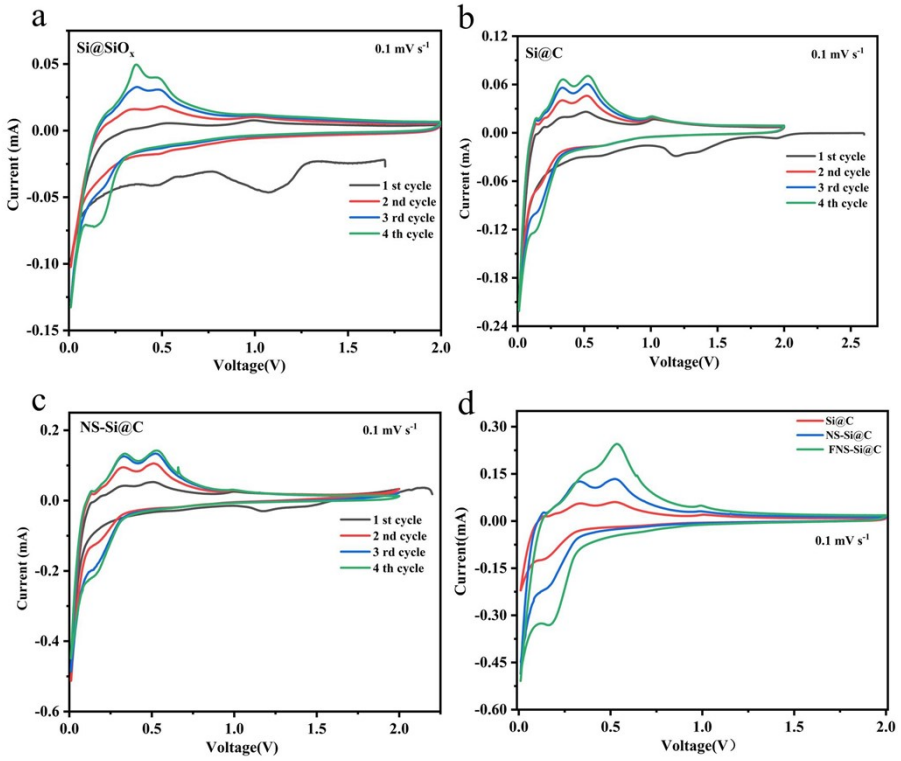

Figure S10. CV curves of electrodes at 0.1 mV s^{-1}. (a) Si@SiO_x; (b) Si@C; (c) NS-Si@C; (d) Comparisons of CV curves of Si@C, NS-Si@C and FNS-Si@C.

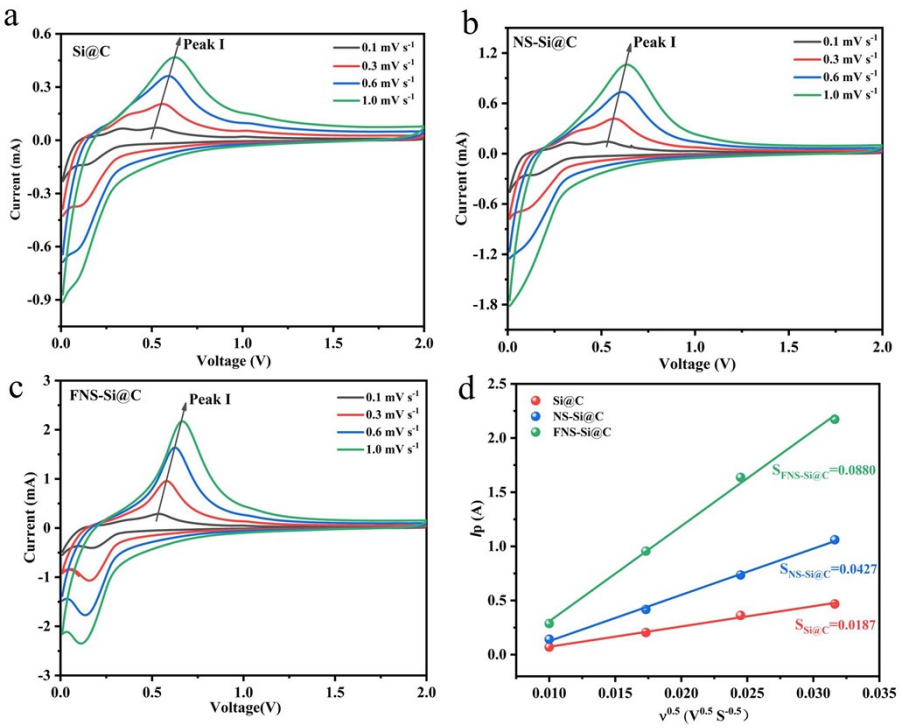

Figure 11. Lithium-ion diffusion coefficients of different electrodes. (a-c) CV curves at different scan rates of Si@C, NS-Si@C and FNS-Si@C electrodes, (d) Linear fits for the anodic peak currents versus square root of the scanning rates of electrodes using Si@C (red), NS-Si@C (blue) and FNS-Si@C (green) from (a-c).

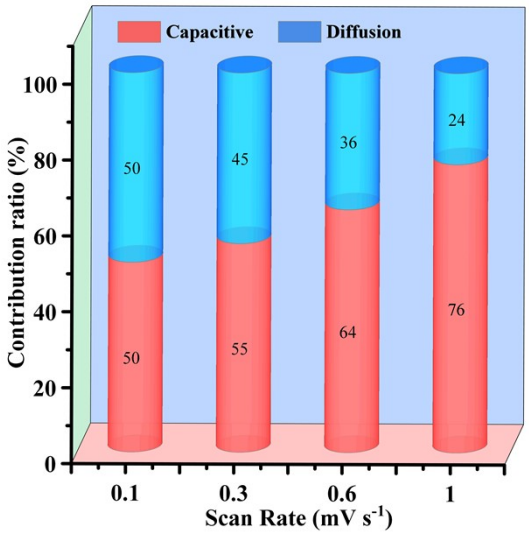

Figure S12. Respective fraction of capacitive and diffusion contribution at various scan rates.

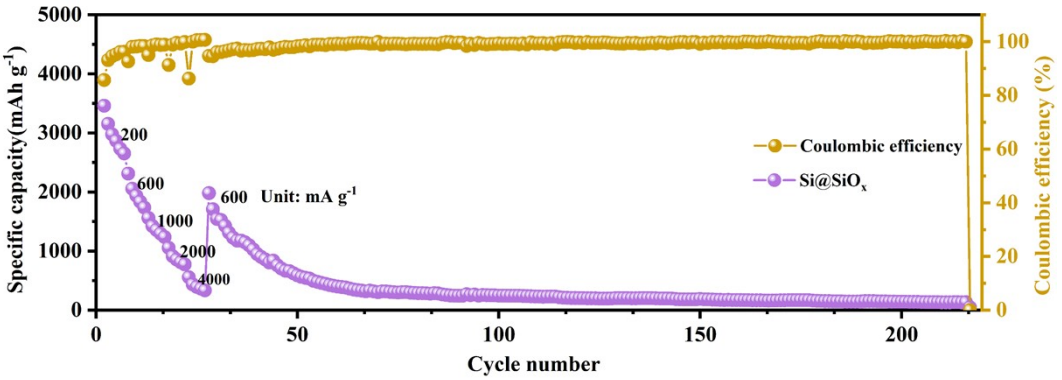

Figure S13. Rate capability and cycle performance of $Si@SiO_x$ electrode.

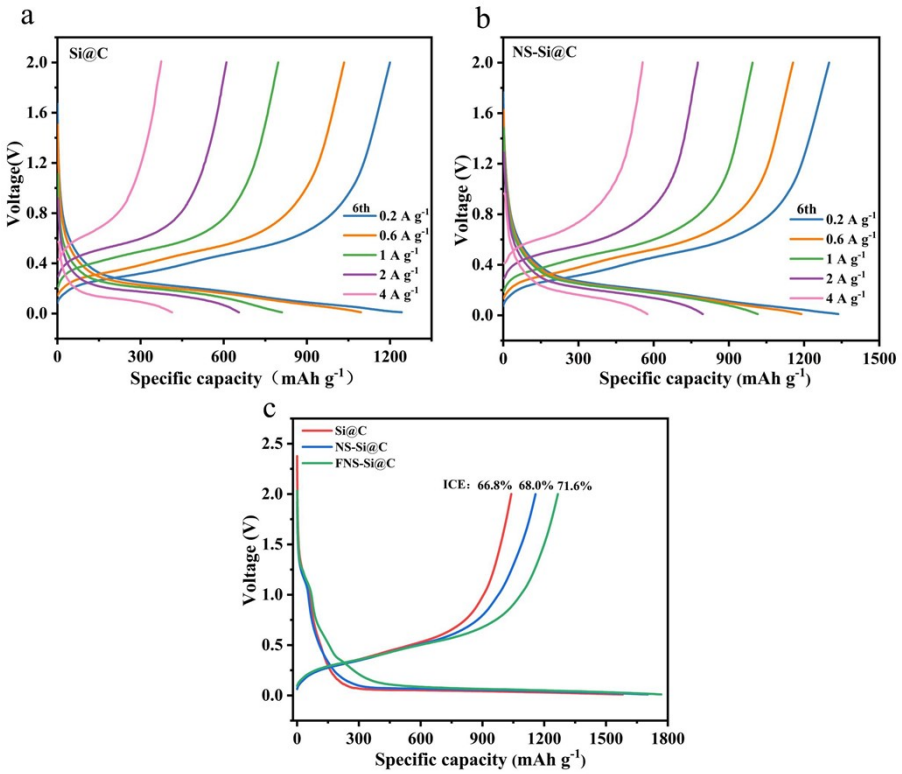

Figure S14. Charge/discharge curves of (a) Si@C and (b) NS-Si@C electrodes. (c) The initial Coulombic efficiency of various electrodes at 0.2 A g^{-1}.

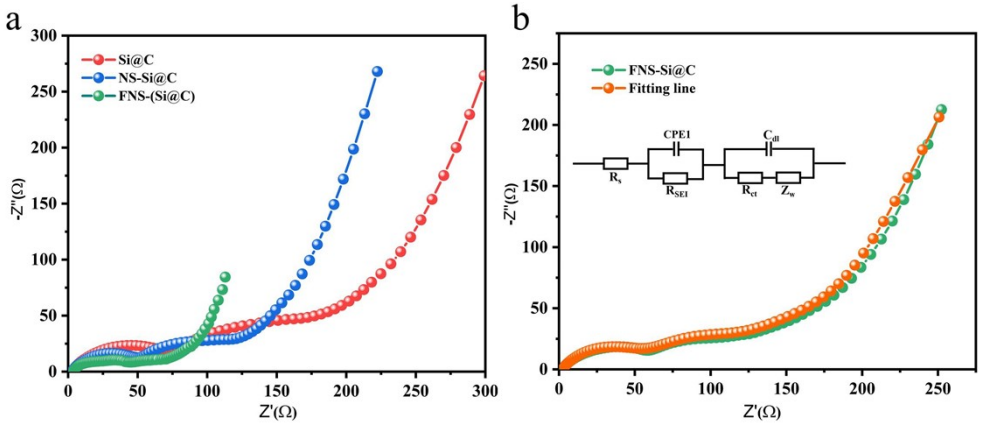

Figure S15. (a) EIS of Si@C, NS-Si@C and FNS-Si@C electrodes. (b) The EIS fitting line of FNS-Si@C electrode (inset is equivalent circuit).

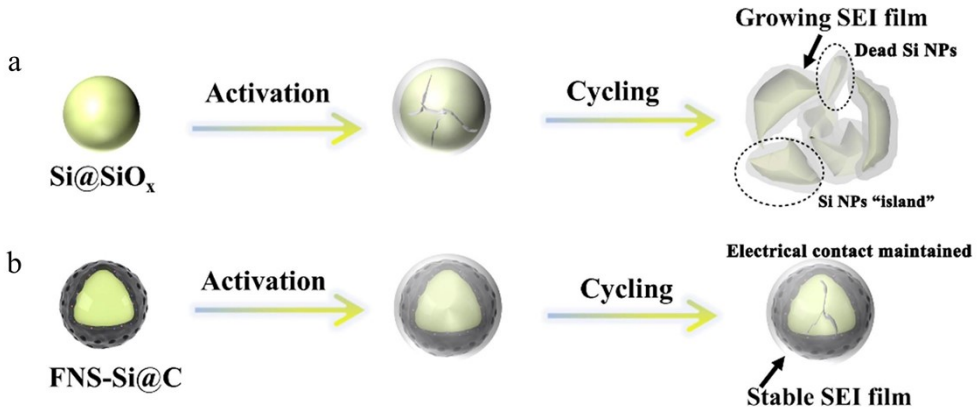

Figure S16. Schematic illustration of the evolution of (a) Si@SiO$_x$; (b) FNS-Si@C electrodes during cycling.

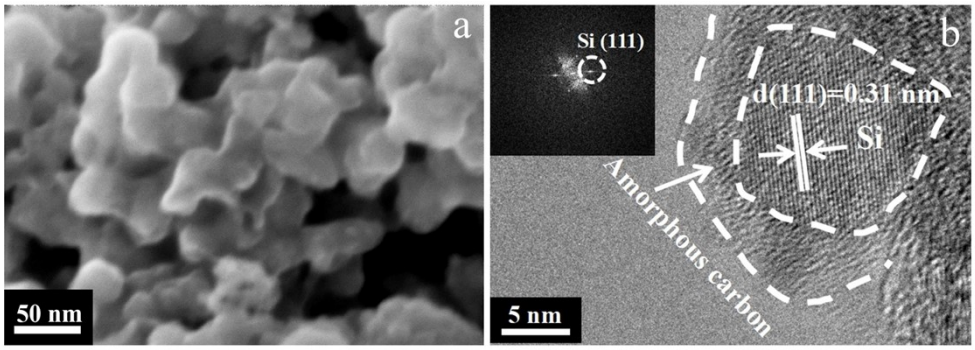

Figure S17. (a) SEM and (b) HR-TEM images of FNS-Si@C composite after cycling.

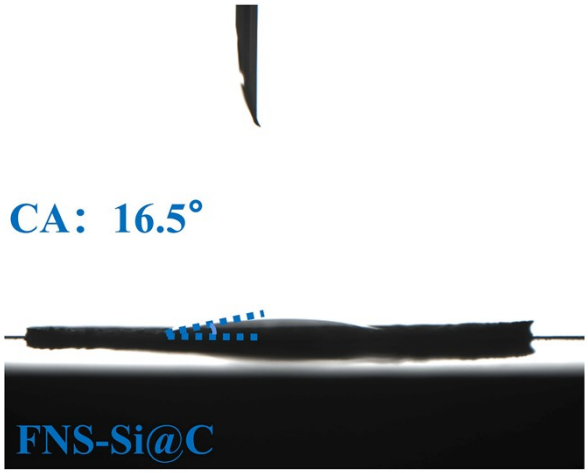

Figure S18. Contact angle measurement of FNS-Si@C electrode.

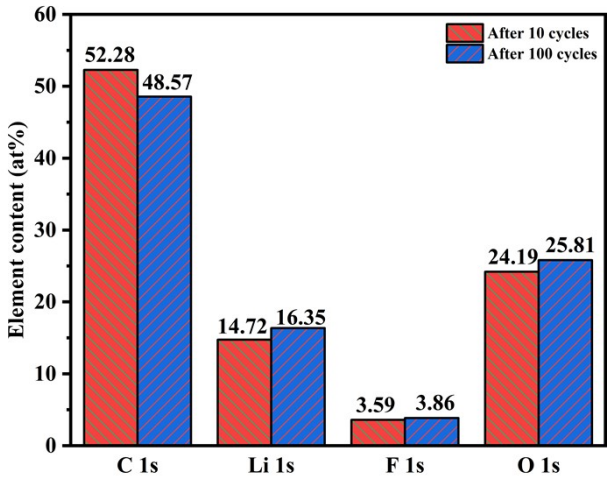

Figure S19. Comparison of the proportion of different elements in FNS-Si@C after 10 cycles and 100 cycles.

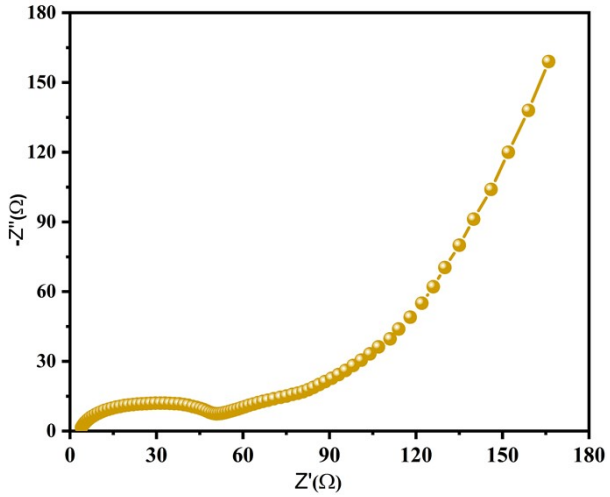

Figure S20. EIS of LFP//FNS-Si@C full cell after cycling.

References

1 F. Weigend and R. Ahlrichs, *Phys. Chem. Chem. Phys.*, 2005, **7**, 3297-3305.

2 Y. Zhao and D. G. Truhlar, *Theor. Chem. Acc.*, 2007, **120**, 215-241.

3 S. Grimme, J. Antony, S. Ehrlich and H. Krieg, *J. Chem. Phys.*, 2010, **132**, 154104.

4 Y. Zhao and D. G. Truhlar, *Acc. Chem. Res.*, 2008, **41**, 157-167.

5 X. Zhang, J. He, L. Zhou, H. Zhang, Q. Wang, B. Huang, X. Lu, Y. Tong and C. Wang, *Adv. Funct. Mater.*, 2021, **31**, 2100443.

6 Z. Li, Y. Zhang, T. Liu, X. Gao, S. Li, M. Ling, C. Liang, J. Zheng and Z. Lin, *Adv. Energy Mater.*, 2020, **10**, 1903110.